Wigner photoemission time delay from endohedral anions

Ashish Kumar and Hari R. Varma[*]

School of Basic Sciences, Indian Institute of Technology Mandi, Kamand, H.P. 175005, India

Pranawa C. Deshmukh

School of Basic Sciences, Indian Institute of Technology Mandi, Kamand, H.P. 175005, India
and Department of Physics, Indian Institute of Technology Madras, Chennai, Tamil Nadu 600036, India

Steven T. Manson

Department of Physics and Astronomy, Georgia State University, Atlanta, Georgia 30303, USA

Valeriy K. Dolmatov

Department of Physics and Earth Science, University of Northern Alabama, Florence, Alabama 35632, USA

Anatoli Kheifets

Research School of Physics and Engineering, The Australian National University, Canberra ACT 0200, Australia

Characteristic features of Wigner photoemission time delay from endohedral anions $A@C_{60}{}^q$ along with their dependence on the anion charge q are unraveled. Specifically, significant enhancement of the time delay in the innermost dipole photoionization channels near threshold is found, owing to the presence of the Coulomb confined resonances (CRs). Moreover, it is shown that interchannel coupling of the inner-shell Coulomb CRs with outer-shell photoionization channels results in resonantly enhanced time delay in the release of the outer-shell photoelectron well above, several hundreds eV, the outer-shell thresholds. It is also demonstrated that, and explained why, photoionization cross sections of the innermost subshells as well as outer subshells (near the inner-subshell threshold) depends only very weakly on the anion charge q, but the dependence of the corresponding time delays on q can be significant. Furthermore, Coulomb CRs are found to emerge in the innermost quadrupole photoionization channels as well, thereby causing considerable time delay in the quadrupole photoemission. These findings are illustrated in calculations of the photoionization of inner and outer subshells of the endohedral anions $Ne@C_{60}{}^{-1}$ and $Ne@C_{60}{}^{-5}$ that were chosen as case studies.

I. INTRODUCTION

The past decade has witnessed a rapid development of attosecond chronoscopy enabling studies of ultrafast electron dynamics in real time (see [1–3] and a recent review article [4] with references therein). The emergence of experimental techniques such as attosecond streaking and RABBITT (reconstruction of attosecond beating by interference of two-photon transitions) has enabled measurements of time delays in the release of photoelectrons from atoms which are normally of the order tens of attoseconds; 1 as $= 10^{-18}$ s [5–9]. These works have stimulated many subsequent experimental and theoretical studies, see, e.g., [10–27] and references therein. Although the time delay appears to be tiny, its knowledge provides opportunities for a deeper understanding of the structure and ionization dynamics of atoms and molecules. For instance, the knowledge of time delay in combination with measured photoionization cross sections, photoelectron angular distributions, along with photoelectron spin asymmetry, allows for a complete photoionization experiment [28], an experiment where the magnitudes and phases of all matrix elements are obtained.

The time delay phenomenon is an example of many-decades-old ideas revived much later. Indeed, the concept of time delay in electron potential scattering, compared to propagation in free space, was introduced more than six decades ago by Eisenbud [29] and Wigner [30]. The predicted time delay phenomenon was shown to be associated with the energy derivative of the elastic scattering phase shift. Since photoionization can be considered as half-scattering, the Eisenbud-Wigner formalism can be applied to the photoionization process as well. There, time delay in the release of a photoelectron from the atom is defined as the difference in the time needed for the maximum of the photoelectron wave packet to arrive to a detector relative to the time taken by a free electron-wave-packet [31]. However, it was not until the pioneering experiment by Shultze *et al.* [7] that the measurement of photoionization time delay has become possible; this has stimulated a great deal of theoretical research. One of the important theoretical findings was the prediction of significant enhancement of the photoionization time delay in the region of Cooper minima as well as in the region of resonances in the photoionization cross section [32–34].

Resonantly enhanced time delay can now be measured experimentally by using tunable narrow band RABBIT [35] or wide band "rainbow" RABBITT [36] techniques. These measurements can provide additional phase information and allow for a complete temporal characterization of the ioniza-

* hari@iitmandi.ac.in

tion dynamics. The phase variation due to interactions between a discrete state and the ionization continua can be used as an additional means for monitoring electron correlations in time.

Currently, much less is known about photoemission time delay in endohedral fullerenes, A@C$_n$ where an "atom-stranger" (A) is captured inside the hollow interior of a carbon fullerene molecule C$_n$ (e.g., C$_{60}$). This is despite importance of these nanoformations to both basic and applied sciences and technologies [37,38]. Because of this importance, they were subject to intense experimental and theoretical spectroscopic studies, see, e.g., [39,40] and references therein. The authors are aware of only Refs. [25,34] studying photoionization time delays of neutral A@C$_{60}$ endohedrals. No comprehensive research has been performed on time delays upon photoionization of A@C$_{60}{}^q$ anions which are other types of nanoformations of interest [41–43].

In the present work, we study photoemission time delays from A@C$_{60}{}^q$ and how they might depend on the anion charge by choosing Ne@C$_{60}{}^q$ with $q = 0, -1$, and -5 as a case study. The choice of Ne is arbitrary except that relativistic effects in Ne are weak which simplifies the study. It is demonstrated that time delays from endohedral anions can be significantly enhanced both near and far above the ionization thresholds. This is due to resonances generally termed the confinement resonances (CRs), which are the intrinsic feature of endohedral atoms, anions, and cations. Furthermore, it is found that the sensitivity of time delays to the charge of the anion is generally weak. The explanation for this will be given below.

Confinement resonances in spectra of endohedral atoms or ions can be classified as follows. First, ordinary CRs which are due to constructive interference between the direct outgoing photoelectron wave and the photoelectron wave scattered off the C_{60} fullerene cage, see, e.g., [44–50] and references therein. Their existence has been experimentally confirmed only very recently [39,40]. Second, correlation CRs, i.e., resonances induced in the spectra of outer subshells by ordinary CRs in inner shell photoionization via interchannel coupling, see, e.g., [49,51,52]. Third, resurrected, or revived, CRs [53] which are, in essence, the same as correlation CRs except that they emerge in valence shell photoionization some hundreds to thousands eV above threshold, specifically, near the ionization thresholds of inner subshells and are also due to interchannel coupling. Normally, CRs die out by a few tens eV above the threshold. Therefore, the emergence of CRs in valence shell photoionization very far above threshold defines resurrected CRs. Fourth, Coulomb CRs [54], i.e., resonances that emerge in the spectra of endohedral anions A@C$_{60}{}^q$. Coulomb CRs are primarily due to a constructive interference of the outgoing photoelectron wave with the wave reflected off the Coulomb potential barrier of an endohedral anion.

The present work illustrates the effects of individual CRs, as well as their combined effect, on time delays from endohedral anions by exploring the $1s$, $2s$, and $2p$ photoemission time delay from Ne@C$_{60}{}^q$ for $q = 0, -1$, and -5. First, we demonstrate the effect of Coulomb CRs on photoemission time delay from the innermost $1s$ subshell of Ne@C$_{60}{}^q$. Then we show the effect of these Coulomb CRs in the $1s$ photoionization channels on photoemission time delays from the valence $2s$ and $2p$ subshells near the $1s$ threshold induced via interchannel coupling. In other words, it is established how

CRs, resurrected in the $2s$ and $2p$ photoemission channels at more than 800 eV above the $2s$ and $2p$ thresholds, affect the corresponding photoemission time delays. Finally, the present work also finds how the quadrupole $1s$ Coulomb CRs affect both the $1s \rightarrow \epsilon d$ photoionization channel and the corresponding quadrupole photoemission time delay.

Atomic units (a.u.) are used throughout the paper unless specified otherwise.

II. THEORY IN BRIEF

In the present work, it is assumed that atom A is positioned at the center of the C$_{60}$ cage; the presence of the C$_{60}$ cage itself is simulated by an attractive spherical potential $V^{\text{cage}}(r)$ of inner radius r_c, thickness Δ, and depth U_0:

$$V^{\text{Cage}}(r) = \begin{cases} -U_0 < 0, & \text{for } r_c \leqslant r \leqslant r_c + \Delta, \\ 0, & \text{otherwise.} \end{cases} \quad (1)$$

The origin of this empirical model can be found in earlier works [44,55], and the model itself has become popular in recent years. In accordance with [55], $r_c = 5.8$ a.u., $\Delta = 1.89$ a.u., and $U_0 = 0.3021$ a.u. $= 8.2$ eV [47]. Furthermore, it is assumed that the excessive negative charge q of C$_{60}{}^q$ is uniformly distributed over the whole spherical surface of the cage. This leads to the emergence of the Coulomb potential $V^q(r)$ in addition to $V^{\text{cage}}(r)$:

$$V^q(r) = \begin{cases} q/(r_c + \Delta), & \text{if } 0 \leqslant r \leqslant r_c + \Delta. \\ q/r, & \text{otherwise.} \end{cases} \quad (2)$$

Accordingly, the C$_{60}{}^q$ cage is to be modeled by the effective potential defined as the sum of $V^q(r)$ and $V^{\text{cage}}(r)$, i.e., $V^{\text{eff}}(r) = V^q(r) + V^{\text{cage}}(r)$.

Thus, the theoretical description of A@C$_{60}{}^q$ photoionization is reduced to the photoionization of the atom A in the presence of the external effective potential $V^{\text{eff}}(r)$. This potential $V^{\text{eff}}(r)$ is added to the atomic potential and the corresponding equations are solved to determine both the wave functions and energies of the ground state configuration of the encapsulated atom and the wave functions of the outgoing photoelectrons. Here the Dirac-Fock approximation is employed for such calculations. In the present work, the relativistic random phase approximation (RRPA) [56,57] is used to calculate the magnitudes and phases of the photoionization matrix elements $D_{n\kappa \rightarrow \varepsilon\bar{\kappa}}$. The RRPA dipole transition matrix element for a transition affected by the absorption of a photon (represented by the operator $Q_J^{(\lambda)}$ with $J = 1$ being the photon angular momentum and $\lambda = 1$ for the electric, as opposed to the magnetic, dipole) from a bound state $n\kappa$ to a continuum state $\varepsilon\bar{\kappa}$ is given by [56]

$$D_{n\kappa \rightarrow \varepsilon\bar{\kappa}} = i^{1-\bar{l}} e^{i\delta_{\bar{\kappa}}} \langle \varepsilon, \bar{\kappa} \| Q_1^{(1)} \| n\kappa \rangle_{\text{RRPA}}. \quad (3)$$

In the above equation, $\kappa = \mp(j + \frac{1}{2})$ for $j = (l \pm \frac{1}{2})$ and $\langle \varepsilon, \bar{\kappa} \| Q_1^{(1)} \| n\kappa \rangle_{\text{RRPA}}$ is the reduced matrix element for the electric dipole transition, with $\bar{\kappa} = -\kappa, \kappa \pm 1$, and $\delta_{\bar{\kappa}}$ is the energy-dependent phase of the single-particle final-state continuum wave function obtained using incoming wave boundary conditions. Since the reduced matrix element is generally complex, the phase of the dipole matrix element,

Eq. (3), is not simply $\delta_{\bar{\kappa}}$, but is given by

$$\delta_{n\kappa \to \varepsilon\bar{\kappa}}(E) = \tan^{-1} \left\{ \frac{\mathrm{Im} D_{n\kappa \to \varepsilon\bar{\kappa}}}{\mathrm{Re} D_{n\kappa \to \varepsilon\bar{\kappa}}} \right\}. \tag{4}$$

The Wigner time delay (in atomic units) in the photoionization channels is then [29,30]

$$\tau_w = \frac{d\delta_{n\kappa \to \varepsilon\bar{\kappa}}(E)}{dE}. \tag{5}$$

A more thorough determination of the time delay would require summations of the photoionization amplitude over all the significant ionization channels. This is essential to evaluate the time delay near the Cooper minimum of the stronger ionization channel where the nominally weaker channel takes over [58]. However, in the present work, we restrict ourselves with only the dominant channel as it retains its dominance across the whole of the resonance.

III. RESULTS AND DISCUSSION

A. Photoionization cross sections

Calculated RRPA results for the dipole $1s$, $2s$, and $2p$ photoionization cross sections of Ne@$C_{60}{}^q$ are shown in Fig. 1.

The depicted data are results of the full RRPA calculation which accounted for interchannel coupling between all dipole possible transitions from Ne : $2p_{3/2} \to (\epsilon d_{5/2}, \epsilon d_{3/2}, \epsilon s_{1/2})$, $2p_{1/2} \to (\epsilon d_{3/2}, \epsilon s_{1/2})$, $2s \to (\epsilon p_{3/2}, \epsilon p_{1/2})$, and $1s \to (\epsilon p_{3/2}, \epsilon p_{1/2})$ transitions. We note that the calculated RRPA results for the $1s$ and $2p$ photoionization cross sections are in excellent agreement with available nonrelativistic results [53,54] (not shown in Fig. 1) obtained
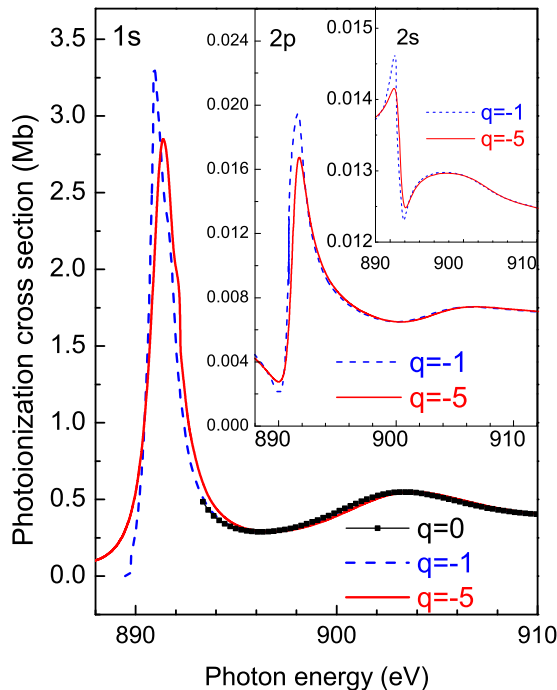

FIG. 1. Photoionization cross section for the $1s^2$, $2s^2$, and $2p^6$ shells of Ne@$C_{60}{}^{-1}$ and Ne@$C_{60}{}^{-5}$, as well as neutral Ne@C_{60} ($q = 0$), as marked.

within the framework of the nonrelativistic random-phase approximation with exchange (RPAE) [59]. This is indicative that relativistic effects are unimportant in the photoionization of Ne@$C_{60}{}^q$.

Below, the photoionization cross sections of each individual $n\ell$ subshell of Ne@$C_{60}{}^q$ are discussed.

1. $1s$ photoionization

The outstanding feature of the $1s$ cross sections of Ne@$C_{60}{}^{-1}$ and Ne@$C_{60}{}^{-5}$ is a strong and sharp near-threshold Coulomb confinement resonance (Coulomb CR) [54]. This Coulomb CR originates from the interference of the outgoing photoelectron wave with the wave scattered off the Coulomb barrier $V^q(r)$ of the Ne@$C_{60}{}^q$ anion. The Coulomb CRs in the Ne@$C_{60}{}^q$ anions are followed by much smaller ordinary CRs at photon energies above 900 eV. Coulomb CRs are naturally absent in the case of neutral Ne@C_{60}, for an obvious reason; this is supported by results plotted in Fig. 1 as well. Since the gross feature of our interest is absent in spectra of neutral endohedral fullerenes, we will focus primarily on results for endohedral anions in further discussion.

An important observation here is that the $1s$ photoionization cross sections of Ne@$C_{60}{}^{-1}$ and Ne@$C_{60}{}^{-5}$ do not differ any dramatically from each other. In other words, the present work finds that increasing the charge of the endohedral anion practically does not affect the corresponding $1s$-photoionization cross sections. At first glance, this finding seems strange. Indeed, the spike in the Coulomb potential at the outer wall of $C_{60}{}^q$ is, obviously, much higher when $q = -5$ compared to $q = -1$. Thus, one would expect a much stronger scattering of the outgoing photoelectron off the Coulomb potential barrier of Ne@$C_{60}{}^{-5}$ than that of Ne@$C_{60}{}^{-1}$, at the same photon energy. This, however, appears not to be the case. The answer to this puzzling observation lies in the fact that the ionization potential (I_{nl}) of a nl subshell of the encapsulated Ne is strongly affected by the negative charge on the fullerene cage—it decreases with increasing q. Thus, $I_{1s} = 889.53$ eV in Ne@$C_{60}{}^{-1}$, but is some 14 eV lower in Ne@$C_{60}{}^{-5}$ where it is found that $I_{1s} = 875.32$ eV. Therefore, the energy of an ϵp photoelectron from Ne@$C_{60}{}^{-5}$ is by about 14 eV greater than that of an ϵp photoelectron from Ne@$C_{60}{}^{-1}$ at a given photon energy. The implication is that the energy distance between the ϵp-photoelectron energy and the peak value of the Coulomb potential barrier is about the same both in Ne@$C_{60}{}^{-5}$ and Ne@$C_{60}{}^{-1}$, at any given value of the photon energy. This results in little difference in scattering of an outgoing photoelectron off the potential of a differently charged fullerene cage. As a consequence, the $1s$-photoionization cross sections of Ne@$C_{60}{}^{-5}$ and Ne@$C_{60}{}^{-1}$ differ from each other only insignificantly.

This phenomenon can also be understood in a slightly different way. Since the excessive negative charge is taken to be spread out uniformly over the outer surface of the confining cage, by Gauss' law, this charge distribution exerts no force inside the sphere. The only effect inside the sphere is to change the potential by a constant amount. Since the $1s$ photoionization takes place well inside the inner radius of the C_{60}, the only effect is the change in I_{1s} in Ne@$C_{60}{}^{-5}$ compared to Ne@$C_{60}{}^{-1}$, as seen above; the wave functions of both

the initial discrete and final continuum states are practically unaffected. The implication is that the effect of placing a negative charge onto the C_{60} surface is to move some of the oscillator strength of the encapsulated atom from the discrete excitation region into the continuum. Correspondingly, the $1s$ cross sections of Ne@C_{60}^{-5}, Ne@C_{60}^{-1}, and the neutral Ne@C_{60} should, with decreasing photon energy, be fairly the same down to the $1s$ threshold of Ne@C_{60}. Then, below this threshold, it is the $1s$ cross sections of Ne@C_{60}^{-5} and Ne@C_{60}^{-1} which are both about the same down to the $1s$ threshold of Ne@C_{60}^{-1}, exactly as Fig. 1 shows.

We note, parenthetically, that the similar phenomenon emerges in the photoionization of positive ions as well, where it was found that the removal of outer-shell electrons does not affect the photoionization cross section of inner shells, as a function of photon energy, except for the change in ionization potential [60].

2. 2p and 2s photoionization

The $2p$ photoionization cross sections $\sigma_{2p}(\omega)$ of Ne@C_{60}^{-1} and Ne@C_{60}^{-5} at photon energies ω, which are more than 800 eV above the Ne $2p$ ionization threshold in both fullerene anions ($I_{2p} \approx 19.5$ eV in Ne@C_{60}^{-1} and 5.5 eV in Ne@C_{60}^{-5}), are each seen to exhibit strong resonance character. At first glance, this is surprising. Indeed, at these photon energies, the energy of an outgoing photoelectron lies so high above the fullerene cage's Coulomb barrier that the photoelectron should be "indifferent" to the presence of both the Coulomb barrier and the potential well. Consequently, the corresponding photoionization cross sections should have been monotonic. Thus, the question arises—where do the resonance structures in $\sigma_{2p}(\omega)$ of Ne@C_{60}^{-1} and Ne@C_{60}^{-5} come from?

For the case of Ne@C_{60}^{-5} the answer was provided in [53]. The strong sharp resonance structure in $\sigma_{2p}(\omega)$ of Ne@C_{60}^{-5} was shown to be due to the interchannel coupling between the Coulomb CR in the inner $1s \to p$ photoionization channel with the outer $2p \to d$ and $2p \to s$ ionization channels. In other words, the strong resonance in $\sigma_{2p}(\omega)$ of Ne@C_{60}^{-5} is a resurrected Coulomb CR, in the terminology of the present paper. As for the other small oscillations in $\sigma_{2p}(\omega)$ of Ne@C_{60}^{-5} at photon energies above 900 eV, they were shown [53] to be induced from the ordinary CRs in the $1s$ photoionization by interchannel coupling of the outer $2p \to d$ and $2p \to s$ channels with the inner $1s \to p$ channel. These resonances in $\sigma_{2p}(\omega)$ of Ne@C_{60}^{-5} are, thus, correlation (or resurrected) CRs, again, in the terminology of the present paper.

This explanation for the resonance structures in $\sigma_{2p}(\omega)$ of Ne@C_{60}^{-5} is equally applicable to the case of $\sigma_{2p}(\omega)$ of Ne@C_{60}^{-1}. Thus, the strong sharp resonance near 890 eV is the resurrected Coulomb CR, whereas the low profile oscillations are correlation CRs all of which are induced in $\sigma_{2p}(\omega)$ by the corresponding resonances in the $1s \to p$ channel via interchannel coupling.

Since all types of CRs in the $1s \to p$ channel were seen to depend only very weakly on the charge q on the fullerene cage, and, for the same reasons, the interchannel coupling matrix elements must also be almost independent of q, then clearly these $1s$ CRs must result in, via interchannel coupling, only insignificantly different effects on $2p$ photoionization for

differing values of q. In other words, $\sigma_{2p}(\omega)$ of Ne@C_{60}^{-1} should differ only minimally from $\sigma_{2p}(\omega)$ of Ne@C_{60}^{-5}. This, indeed, is clearly demonstrated in Fig. 1.

With respect to the $2s$ photoionization, the present study reveals that, similar to the $2p$ photoionization, $\sigma_{2s}(\omega)$ of Ne@C_{60}^{-1} and Ne@C_{60}^{-5} are dominated by a strong sharp resonance which is followed by weak oscillations with increasing photon energy. Clearly the strong sharp resonance in $\sigma_{2s}(\omega)$ is the resurrected Coulomb CR, which comes, via interchannel coupling, from the Coulomb CR in the $1s \to p$ channel, whereas other oscillatory structures in $\sigma_{2s}(\omega)$ are induced by ordinary CRs in the $1s \to p$ channel. Indeed, a trial calculation showed that the exclusion of the $1s \to p$ transition from interchannel coupling with the $2s$ transitions from the RRPA calculation eliminates any resonance structure from $\sigma_{2s}(\omega)$, making the latter be a monotonic function of energy (not shown).

It is of interest to note that the $1s \to \epsilon p$ channel affects the $2p$ photoionization much more strongly than it affects the $2s$ photoionization. This can be understood from the fact that, when there are multiple subshell cross sections energetically allowed at a given photon energy, interchannel coupling causes mixing among them. As a result, channels with small cross sections can be significantly enhanced by this coupling. Furthermore, the percentage of enhancement depends upon the relative magnitudes of the two cross sections [61,62]. In the present case, $\sigma_{2p}(\omega) \gg \sigma_{2s}(\omega)$ near their own thresholds [61]. However, $\sigma_{2p}(\omega) \ll \sigma_{2s}(\omega)$ in the vicinity of the $1s$ threshold [61]. This is because ns photoionization cross sections fall off, at high energies, which are far above thresholds, as $\varepsilon^{-7/2}$, while np photoionization cross sections fall off as $\varepsilon^{-9/2}$. Hence, eventually, $\sigma_{ns}(\omega)$ will always dominate $\sigma_{np}(\omega)$ very far above their thresholds [63]. As a result, we expect more prominent resurrected Coulomb CRs, as well as resurrected ordinary CRs, to emerge in $\sigma_{2p}(\omega)$ than in $\sigma_{2s}(\omega)$, exactly as the RRPA calculations demonstrate.

B. Phases of matrix elements and time delays

1. 1s and 2s photoionization

Calculated RRPA results indicate that phases of the $1s \to \epsilon p_{3/2}$ and $1s \to \epsilon p_{1/2}$ photoionization amplitudes are practically identical, and the same is true for the $2s \to \epsilon p_{3/2}$ and $2s \to \epsilon p_{1/2}$ photoionization amplitudes as well. This is not surprising since Ne is so low in Z that relativistic effects are unimportant. For this reason we present data (by arbitrary choice) for only $1s \to \epsilon p_{3/2}$ and $2s \to \epsilon p_{3/2}$ transitions. The corresponding data are plotted in Fig. 2.

The key result here is the emergence of the strong sharp resonance below 900 eV and a rather diffuse higher energy resonance (above 900 eV) in the $\phi_{1s \to \epsilon p_{3/2}}$ and $\phi_{2s} \to \epsilon p_{3/2}$ phases. These resonances are due to the Coulomb and ordinary confinement resonances in the $1s \to \epsilon p_{3/2}$ channel which re-emerge in the $2s \to \epsilon p_{3/2}$ channel via interchannel coupling between the $1s \to \epsilon p_{3/2}$ and $2s \to \epsilon p_{3/2}$ transitions. This is evident from the comparison of the positions of these resonances in the corresponding cross sections (Fig. 1) and phases (Fig. 2). The present work, thus, establishes how CRs in inner-shell photoionization transition transfer, via interchannel coupling, to phases of outer-shell matrix elements. In terms of
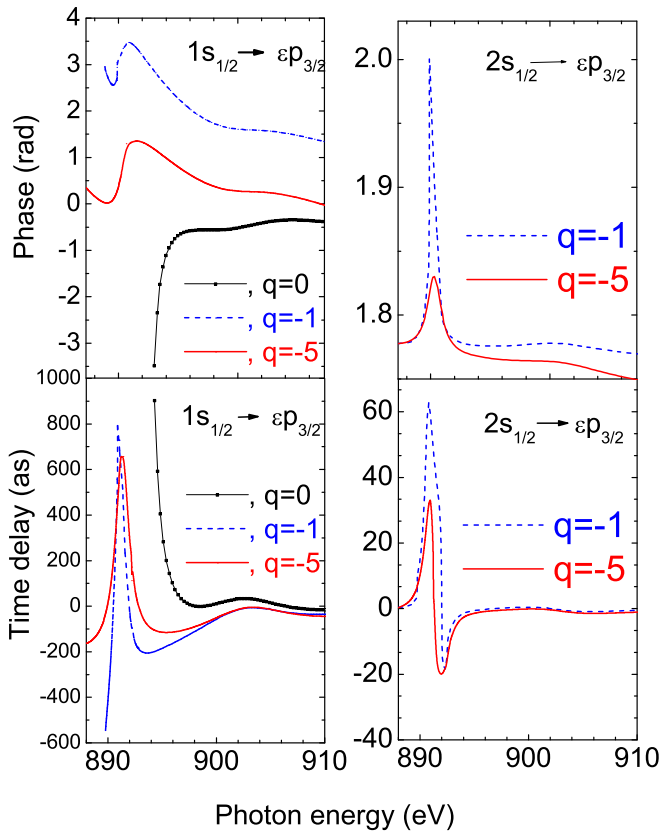
FIG. 2. Calculated RRPA data (with full account of coupling channels) for phases of $1s \to \epsilon p_{3/2}$ and $2s \to \epsilon p_{3/2}$ matrix elements and corresponding time delays for $1s$ and $2s$ photoionization of Ne@C_{60}^q ($q = 0, -1,$ and -5), as marked.

the present case, the strong sharp resonance in $\phi_{2s \to \epsilon p_{3/2}}$ is the resurrected Coulomb CR, arising from the Coulomb CR in the $1s$ channel, whereas the weak oscillations are resurrected ordinary CRs.

The rapid changes in the phase $\phi_{1s \to \epsilon p_{3/2}}$, due to Coulomb CRs, and in the phase $\phi_{2s \to \epsilon p_{3/2}}$, due to the resurrected Coulomb CR, are seen to result in the significant resonant enhancement of the respective time delays. Indeed, time delay reaches several hundred attoseconds in the $1s$ photoionization and tens attoseconds in the $2s$ photoionization. As for the influence of the ordinary CRs (near 905 eV) on the calculated phases and time delays, although the impact is present, it is negligible compared to the impact of the Coulomb CRs.

The calculated data for the $1s$ and $2s$ photoionization time delays τ_{1s} and τ_{2s} reveal another important feature of this physical quantity compared to the photoionization cross sections and phases. It is as follows. The calculated photoionization cross sections differ only insignificantly between the cases of the differently charged anions. The same is true for phases of the photoionization matrix elements, on the *absolute scale*; e.g., the largest difference between $\phi_{2s \to \epsilon p_{3/2}}^{q=-1}$ and $\phi_{2s \to \epsilon p_{3/2}}^{q=-5}$, see Fig. 2, is about 10%. In contrast to the cross sections and phases, the calculated time delays may differ significantly between the two cases. This is because time delay is proportional to *energy derivative* of the phase rather than to its value. Therefore, a small difference, on an *absolute*

scale, between the phases of photoionization matrix elements for differently charged anions, may result in significant difference between the corresponding photoionization time delays. Indeed, in the case studies of the present paper, the energy variations of the phases $\phi_{1s \to \epsilon p_{3/2}}^{q=-1}$ and $\phi_{2s \to \epsilon p_{3/2}}^{q=-1}$ in the Coulomb CR energy region are somewhat sharper than the energy variations of $\phi_{1s \to \epsilon p_{3/2}}^{q=-5}$ and $\phi_{2s \to \epsilon p_{3/2}}^{q=-5}$. Whereas this difference would not (and does not) significantly affect the corresponding photoionization cross sections, it should (and does) induce noticeable differences in photoionization time delays between τ_{1s}^{-1} and τ_{1s}^{-5}, as well as between τ_{2s}^{-1} and τ_{2s}^{-5}.

The present work, thus, demonstrates that photoionization time delay is a physical quantity which is more sensitive to the anion charge than a photoionization cross section or the phase of a photoionization matrix element itself.

Finally, it is of interest to note that the Coulomb CRs in the $1s \to \epsilon p_{3/2}$ transition affect the time delay $\tau_{1s \to \epsilon p_{3/2}}$ qualitatively differently as compared to the effect of these resonances on $\tau_{2s \to \epsilon p_{3/2}}$. Specifically, the Coulomb CRs in the $1s \to \epsilon p_{3/2}$ transition result in a mostly positive increase of $\tau_{1s \to \epsilon p_{3/2}}$, while they cause $\tau_{2s \to \epsilon p_{3/2}}$ to exhibit strongly positive and strongly negative excursions in the resonance region.

2. 2p photoionization

In our further discussion of the $2p$ photoionization, we focus on only the $2p_{3/2} \to \epsilon d_{5/2}$ channel. This is because the transition $2p_{1/2} \to \epsilon d_{3/2}$ differs little from the $2p_{3/2} \to \epsilon d_{5/2}$ transition (in view of the weakness of relativistic effects in this case) and the major oscillator strength is concentrated in the $2p \to \epsilon d$ transitions rather than in $2p \to \epsilon s$.

The calculated RRPA phases $\phi_{\epsilon d_{5/2}}$ of the $2p_{3/2} \to \epsilon d_{5/2}$ matrix elements for the cases of the Ne@C_{60}^{-1} and Ne@C_{60}^{-5} photoionization are depicted in Fig. 3.

As seen, the calculated phases are dominated by the strong sharp resonance below 900 eV, and a resonance of low intensity above 900 eV. It now goes without saying that the sharp resonance in $\phi_{\epsilon d_{5/2}}$ is induced by the Coulomb CR, whereas low profile oscillations by ordinary CRs in the $1s \to \epsilon p$ channel. Naturally, the resurrected CRs in the phase $\phi_{\epsilon d_{5/2}}$ of the $2p_{3/2} \to \epsilon d_{5/2}$ matrix element must show up in the time delay $\tau_{2p_{3/2} \to \epsilon d_{5/2}}$ of the $2p_{3/2} \to \epsilon d_{5/2}$ photoemission as well, leading to a significant enhancement of the time delay. This is clearly demonstrated by calculated $\tau_{2p_{3/2} \to \epsilon d_{5/2}}$ depicted in Fig. 3 as well.

As in the cases of the $1s$ and $2s$ photoionization, one can see that the value of $\phi_{\epsilon d_{5/2}}^{q=-1}$ in the case of the Ne@C_{60}^{-1} photoionization does not differ significantly, on an absolute scale, from $\phi_{\epsilon d_{5/2}}^{q=-5}$ upon the Ne@C_{60}^{-5} photoionization, but the energy dependence of the resurrected CR in $\phi_{\epsilon d_{5/2}}^{q=-1}$ is somewhat sharper than in $\phi_{\epsilon d_{5/2}}^{q=-5}$. This results in a much greater *magnitude* of $\tau_{2p_{3/2} \to \epsilon d_{5/2}}^{q=-1}$ compared to $\tau_{2p_{3/2} \to \epsilon d_{5/2}}^{q=-5}$ at the minima and somewhat greater $\tau_{2p_{3/2} \to \epsilon d_{5/2}}^{q=-1}$ than $\tau_{2p_{3/2} \to \epsilon d_{5/2}}^{q=-5}$ at maxima in both graphs for time delays, whereas they are fairly close to each other at other energies. These data support the conclusion of the previous section that the time delay is more sensitive to the charge of an anion than the photoionization cross section or the phase of the matrix element itself.
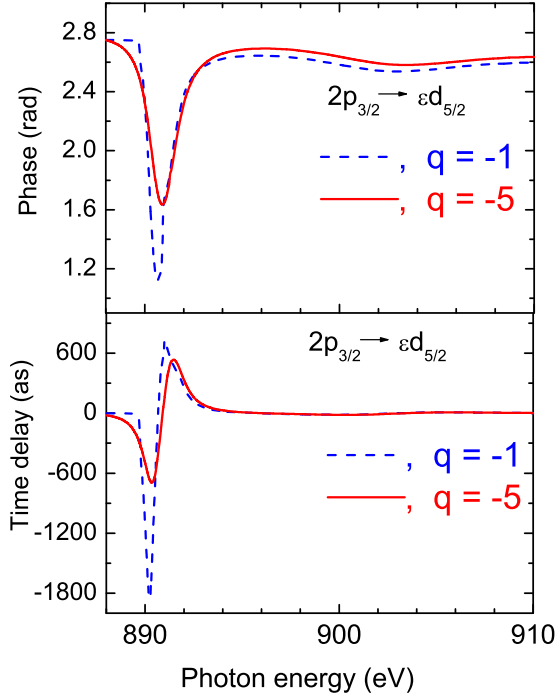
FIG. 3. Calculated RRPA data for the phase of the $2p_{3/2} \rightarrow \epsilon d_{5/2}$ matrix elements and the corresponding time delay for $2p$ photoionization of Ne@C_{60}^q ($q = -1$ and -5), as marked.

It is interesting to note that the resonances in $\phi_{\epsilon d_{5/2}}$ of the $2p_{3/2} \rightarrow \epsilon d_{5/2}$ matrix element are the window-type resonances in contrast to the same resurrected CRs in the phase of the $2s \rightarrow \epsilon p_{3/2}$ transition (cf. Figs. 2 and 3). Indeed, whereas the CRs cause $\tau_{2s_{1/2} \rightarrow \epsilon p_{3/2}}$ to first rise and then fall, the time delay $\tau_{2p_{3/2} \rightarrow \epsilon d_{5/2}}$ of $2p_{3/2} \rightarrow \epsilon d_{5/2}$ photoionization first sharply falls and then sharply rises with increasing energy. The most important difference between $\tau_{2p_{3/2} \rightarrow \epsilon d_{5/2}}$ and $\tau_{2s_{1/2} \rightarrow \epsilon p_{3/2}}$, however, lies in an impressive difference in their magnitudes which may differ by about two orders of magnitude at their "maxima." Indeed, e.g., for $q = -1$, $|\tau_{2p_{3/2} \rightarrow \epsilon d_{5/2}}| \approx 2000$ as at ≈ 890 eV, whereas $|\tau_{2s_{1/2} \rightarrow \epsilon p_{3/2}}| \approx |-20|$ as at the same energy. This demonstrates a qualitatively different impact of the $1s \rightarrow \epsilon p$ transitions on the phase and time delay of the $2p \rightarrow \epsilon d$ transitions compared to that on the phase and time delay of the $2s \rightarrow \epsilon p$ transitions. The overall greater resonance enhancement of $\tau_{2p_{3/2} \rightarrow \epsilon d_{5/2}}$ compared to $\tau_{2s_{1/2} \rightarrow \epsilon p_{3/2}}$ is a direct consequence of the quantitative differences in the details of the effect of the interchannel coupling of the $1s \rightarrow \epsilon p$ channel on the $2p \rightarrow \epsilon d$ channel compared to the effect on $2s \rightarrow \epsilon p$ at $\epsilon \sim I_{1s} \gg I_{2s}$ and I_{2p}.

C. 1s electric-quadrupole photoionization

It is now well known that, at keV-photon energies, the dipole approximation alone is not sufficient for an adequate understanding of photoelectron angular distributions which are often strongly affected by electric-quadrupole transitions as well (see, e.g., [64,65] and references therein). Since time delay is an angular-dependent entity as well [24], it brings up the necessity of studying time delay in electric-quadrupole photoemission, too.
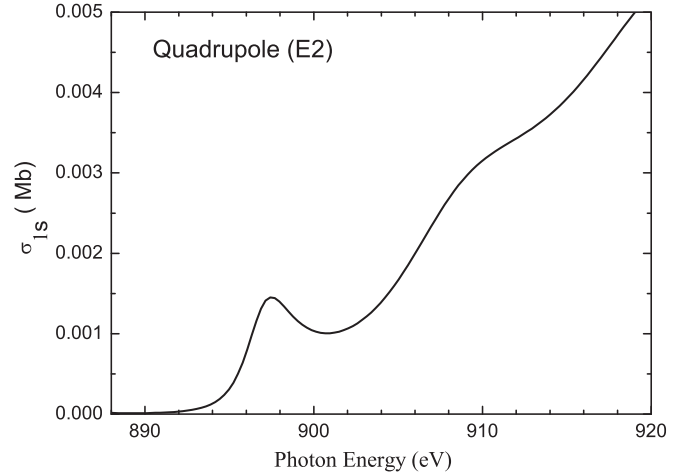

FIG. 4. Electric-quadrupole photoionization cross section of the $1s$ subshell of Ne@C_{60}^{-5}.

Below, the trends in the electric-quadrupole photoionization are revealed and demonstrated using the example of the $1s$ photoionization of Ne@C_{60}^{-5} which is an arbitrary choice of one of the two anions of interest (Ne@C_{60}^{-1} and Ne@C_{60}^{-5}) in the present paper.

The calculated $1s$ electric-quadrupole photoionization cross section σ_{1s}^Q for Ne@C_{60}^{-5} is depicted in Fig. 4 (interchannel coupling between all possible electric-quadrupole one-electron $1s$ transitions has been accounted for in the calculation).

One can see that σ_{1s}^Q is both qualitatively and quantitatively different from the corresponding dipole photoionization cross section σ_{1s}^D in the energy region considered, and this occurs for two reasons. First, $\sigma_{1s}^Q \ll \sigma_{1s}^D$ because σ_{1s}^Q is proportional to a squared product of the photon wave number and the Bohr radius $(ka_0)^2$; this product is small, about 0.05, at these energies. Second, the quadrupole ϵd photoelectron wave (arising from the quadrupole $1s \rightarrow \epsilon d$ transition) experiences a larger centrifugal barrier than the dipole ϵp wave. This is particularly relevant to the near threshold energy region in the endohedral anion photoionization, where the centrifugal potential barrier and the positive Coulomb potential barrier of the anion both hamper the penetration of low-energy photoelectrons into the inner region of the atom. This makes the overlap between the $1s$ and the ϵd wave functions, due to the quadrupole transition, much smaller than the overlap between the $1s$ and ϵp wave functions (due to the dipole transition). Thus, it is clear why there are characteristic differences between the dipole and quadrupole photoionization in the threshold region of the $1s$ channel.

The calculated phase $\phi_{\epsilon d_{5/2}}$ and time delay $\tau_{1s \rightarrow \epsilon d_{5/2}}$ of the $1s \rightarrow \epsilon d_{5/2}$ photoionization channel are depicted in Fig. 5 ($\phi_{\epsilon d_{3/2}}$ and $\tau_{1s \rightarrow \epsilon d_{3/2}}$ for the $1s \rightarrow \epsilon d_{3/2}$ channel are virtually identical to those for the $1s \rightarrow \epsilon d_{5/2}$ channel, for which reason they are not presented separately).

Note that the confinement resonances are much more prominent and sharper in the phase $\phi_{\epsilon d_{5/2}}$ than in σ_{1s}^Q. These sharp variations, in turn, result in a resonance increase of time delay $\tau_{1s \rightarrow \epsilon d_{5/2}}$ in the quadrupole photoionization channel,
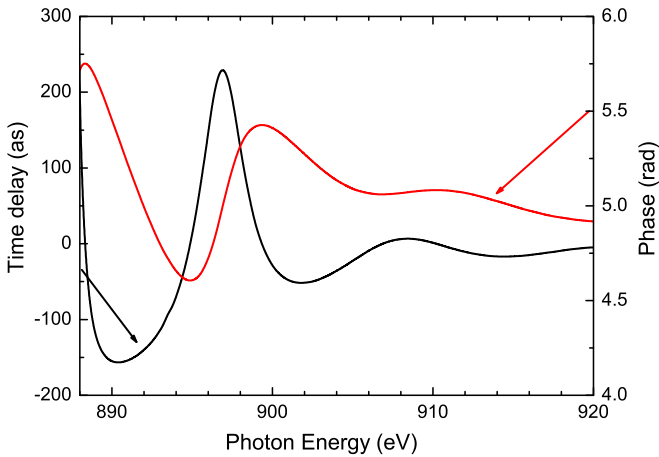
FIG. 5. Time delay (black, left scale) and phase (red, right scale) for the $1s \rightarrow \epsilon d_{5/2}$ electric-quadrupole photoionization channel.

which varies from hundreds of attoseconds negative to positive in the energy region of the resonances.

The presented result is a spectacular finding which uncovers that large time delays can be generated even though the resonance cross sections are quite small.

IV. CONCLUSIONS

Using the Ne atom encapsulated in a negatively charged C_{60} as an example, calculations, employing the RRPA, have shown that Wigner time delays in photoionization of endohedral anions are dramatically enhanced at photon energies near thresholds of inner(most) subshells of the encapsulated atom, primarily due to Coulomb CRs in the inner-shell photoionization channel. These Coulomb CRs, in turn, are due to the Coulomb potential barrier caused by the negative charge on the fullerene cage. Furthermore, the Coulomb and ordinary CRs in the $1s$ channel also are seen to affect the Wigner time delays in the photoionization of the outer $2s$ and $2p$ subshells in the vicinity of the inner-shell threshold, an effect brought about by interchannel coupling.

It has also been found that, and explained why, the gross CR structures in the photoionization *cross section* and *phases* of the matrix elements of endohedral anions near inner subshells depend relatively weakly on the charge on the fullerene cage but photoionization *time delays* may not. For photoionization cross sections, this is because an increase in the Coulomb potential barrier with increasing charge on the shell is compensated by the decrease of the ionization potentials of the subshells of the encapsulated atom, so that, at a given energy of the photon, photoelectron energy is at about the same height above the peak of the Coulomb potential barrier regardless of the charge on the fullerene cage. The

greater sensitivity of time delay to an ionic charge occurs because time delay is defined by the energy derivative of the phase of the matrix element. Therefore, some differences in the energy dependence of the phases between photoionization of differently charged anions, on the background of only tiny numerical differences between the phases, may cause (and did cause in the present study) significant differences in time delays between photoionization of differently charged fullerene anions.

Effects similar to those found for dipole photoionization are found to emerge in electric-quadrupole photoionization as well.

The important fact here is that there is nothing special about the $Ne@C_{60}{}^q$; the time delay effects found should be exhibited for essentially any atom enclosed in any negatively charged fullerene. Thus, although only results for $Ne@C_{60}{}^{-1}$ and $Ne@C_{60}{}^{-5}$ have been presented, the explanation of the the various effects make it clear that these will be general phenomena. Furthermore, the present investigation, along with previous studies [34], suggests that photoionization time delay studies of endohedral systems might be of significant interest, especially in the region of the various genres of confinement oscillations. Experimentally, these resonantly enhanced time delays could be studied using tunable narrow band RABBIT [35] or wide band "rainbow RABBITT" [36] techniques. Both techniques require the use of an additional IR laser probe. This, in turn, requires evaluation of the correspondingly induced so-called continuum-continuum (CC) [66] or the Coulomb laser coupling [21] corrections to the *actual* Wigner time delay to interpret *experimental* data. The latter, thus, differ, to some degree, from the actual Wigner time delay. Hence, the study of time delay can be divided into two independent parts. The first one is the basic study which explores the Wigner time delay as a pure phenomenon which exists by itself without reference to an external observer. It is this study which has been the aim of the present paper. The second part is a practical calculation of the CLC corrections to facilitate comparison of the measured time delay with theoretical predictions. While such calculation is of obvious importance to experimentalists, it constitutes an independent study which goes beyond the scope of the present paper.

[1] P. M. Paul, E. S. Toma, P. Breger, G. Mullot, F. Auge, Ph. Balcou, H. G. Muller, and P. Agostini, Science **292**, 1689 (2001).

[2] A. Baltuska, Th. Udem, M. Uiberacker, M. Hentschel, E. Goulielmakis, Ch. Gohle, R. Holzwarth, V. S. Yakovlev, A. Scrinzi, T. W. Hänsch, and F. Krausz, Nature (London) **421**, 611 (2003).

[3] P. Eckle, M. Smolarski, P. Schlup, J. Biegert, A. Staudte, M. Schöffler, H. G. Muller, R. Dörner, and U. Keller, Nat. Phys. **4**, 565 (2008).

[4] R. Pazourek, S. Nagele, and J. Burgdörfer, Rev. Mod. Phys. **87**, 765 (2015).

[5] K. Klunder, J. M. Dahlstrom, M. Gisselbrecht, T. Fordell, M. Swoboda, D. Guénot, P. Johnsson, J. Caillat, J. Mauritsson, A. Maquet, R. Taieb, and A. LHuillier, Phys. Rev. Lett. **106**, 143002 (2011).

[6] D. Guénot, K. Klunder, C. L. Arnold, D. Kroon, J. M. Dahlstrom, M. Miranda, T. Fordell, M. Gisselbrecht, P. Johnsson, J. Mauritsson, E. Lindroth, A. Maquet, R. Taieb, A. LHuillier, and A. S. Kheifets, Phys. Rev. A **85**, 053424 (2012).

[7] M. Schultze *et al.*, Science **328**, 1658 (2010).

[8] C. Palatchi, J. M. Dahlström, A. S. Kheifets, I. A. Ivanov, D. M. Canaday, P. Agostini, and L. F. DiMauro, J. Phys. B **47**, 245003 (2014).

[9] D. Guénot, D. Kroon, E. Balogh, E. W. Larsen, M. Kotur, M. Miranda, T. Fordell, P. Johnsson, J. Mauritsson, M. Gisselbrecht, K. Varju, C. L. Arnold, T. Carette, A. S. Kheifets, E. Lindroth, A. L. Huillier, and J. M. Dahlström, J. Phys. B **47**, 245602 (2014).

[10] V. S. Yakovlev, J. Gagnon, N. Karpowicz, and F. Krausz, Phys. Rev. Lett. **105**, 073001 (2010).

[11] A. S. Kheifets and I. A. Ivanov, Phys. Rev. Lett. **105**, 233002 (2010).

[12] M. Ivanov and O. Smirnova, Phys. Rev. Lett. **107**, 213605 (2011).

[13] R. Pazourek, J. Feist, S. Nagele, and J. Burgdorfer, Phys. Rev. Lett. **108**, 163001 (2012).

[14] C.-H. Zhang and U. Thumm, Phys. Rev. A **84**, 033401 (2011).

[15] L. R. Moore, M. A. Lysaght, J. S. Parker, H. W. van der Hart, and K. T. Taylor, Phys. Rev. A **84**, 061404 (2011).

[16] A. S. Kheifets, Phys. Rev. A **87**, 063404 (2013).

[17] J. M. Dahlström, T. Carette, and E. Lindroth, Phys. Rev. A **86**, 061402 (2012).

[18] I. A. Ivanov, A. S. Kheifets, and V. V. Serov, Phys. Rev. A **86**, 063422 (2012).

[19] T. Carette, J. M. Dahlström, L. Argenti, and E. Lindroth, Phys. Rev. A **87**, 023420 (2013).

[20] J. Su, H. Ni, A. Becker, and A. Jaron-Becker, Phys. Rev. A **87**, 033420 (2013).

[21] R. Pazourek, S. Nagele, and J. Burgdörfer, Faraday Discuss. **163**, 353 (2013).

[22] J. M. Dahlström and E. Lindroth, J. Phys. B **47**, 124012 (2014).

[23] A. Maquet, J. Caillat, and R. Taeb, J. Phys. B **47**, 204004 (2014).

[24] J. Wätzel, A. S. Moskalenko, Y. Pavlyukh, and J. Berakdar, J. Phys. B **48**, 025602 (2015).

[25] T. Barillot, C. Cauchy, P.-A. Hervieux, M. Gisselbrecht, S. E. Canton, P. Johnsson, J. Laksman, E. P. Mansson, J. M. Dahlström, M. Magrakvelidze, G. Dixit, M. E. Madjet, H. S. Chakraborty, E. Suraud, P. M. Dinh, P. Wopperer, K. Hansen, V. Loriot, C. Bordas, S. Sorensen, and F. Lépine, Phys. Rev. A **91**, 033413 (2015).

[26] M. Magrakvelidze, M. E. Madjet, G. Dixit, M. Ivanov, and H. S. Chakraborty, Phys. Rev. A **91**, 063415 (2015).

[27] A. S. Kheifets, S. Saha, P. C. Deshmukh, D. A. Keating, and S. T. Manson, Phys. Rev. A **92**, 063422 (2015).

[28] N. A. Cherepkov and S. K. Semenov, J. Phys. B **37**, 1267 (2004).

[29] L. Eisenbud, Ph.D. thesis, Princeton University, 1948.

[30] E. P. Wigner, Phys. Rev. **98**, 145 (1955).

[31] F. T. Smith, Phys. Rev. **118**, 349 (1960).

[32] G. Dixit, H. S. Chakraborty, and M. El.-A. Madjet, Phys. Rev. Lett. **111**, 203003 (2013).

[33] S. Nagele, R. Pazourek, M. Wais, G. Wachter, and J. Burgdorfer, J. Phys.: Conf. Ser. **488**, 012004 (2014).

[34] P. C. Deshmukh, A. Mandal, S. Saha, A. S. Kheifets, V. K. Dolmatov, and S. T. Manson, Phys. Rev. A **89**, 053424 (2014).

[35] M. Kotur, D. Guénot, A. Jiménez-Galán, D. Kroon, E. W. Larsen, M. Louisy, S. Bengtsson, M. Miranda, J. Mauritsson, C. L. Arnold, S. E. Canton, M. Gisselbrecht, T. Carette, J. M. Dahlström, E. Lindroth, A. Maquet, L. Argenti, F. Martín, and A. L. Huillier, Nat. Commun. **7**, 10566 (2016).

[36] L. Argenti, V. Gruson, L. Barreau, A. Jimenez-Galan, F. Risoud, J. Caillat, A. Maquet, B. Carre, F. Lepetit, J.-F. Hergott, T. Ruchon, R. Taíeb, F. Martíin, and P. Salieres, Bull. Am. Phys. Soc. G8001A (2016).

[37] H. Shinohara, Rep. Prog. Phys. **63**, 843 (2000).

[38] L. Forre and L. Mihaly, Rep. Prog. Phys. **64**, 649 (2001).

[39] A. L. D Kilcoyne, A. Aguilar, A. Möller, S. Schippers, C. Cisneros, G. AlnaWashi, N. B. Aryal, K. K. Baral, D. A. Esteves, C. M. Thomas, and R. A. Phaneuf, Phys. Rev. Lett. **105**, 213001 (2010).

[40] R. A. Phaneuf, A. L. D. Kilcoyne, N. B. Aryal, K. K. Baral, D. A. Esteves-Macaluso, C. M. Thomas, J. Hellhund, R. Lomsadze, T. W. Gorczyca, C. P. Ballance, S. T. Manson, M. F. Hasoglu, S. Schippers, and A. Möller, Phys. Rev. A **88**, 053402 (2013).

[41] L. Udvari, AIP Conf. Proc. **44**, 187 (2000).

[42] P. Jakes, B. Goedde, M. Wailblinger, N. Weiden, K.-P. Dinse, and A. Weidinger, AIP Conf. Proc. **44**, 174 (2000).

[43] R. C. Bilodeau, N. D. Gibson, C. W. Walter, D. A. Esteves-Macaluso, S. Schippers, A. Mueller, R. A. Phaneuf, A. Aguilar, M. Hoener, J. M. Rost, and N. Berrah, Phys. Rev. Lett. **111**, 043003 (2013).

[44] M. J. Puska and R. M. Nieminen, Phys. Rev. A **47**, 1181 (1993).

[45] A. S. Baltenkov, Phys. Lett. A **254**, 203 (1999).

[46] J.-P. Connerade, V. K. Dolmatov, and S. T. Manson, J. Phys. B **33**, 2279 (2000).

[47] V. K. Dolmatov, A. S. Baltenkov, J.-P. Connerade, and S. T. Manson, Rad. Phys. Chem. **70**, 417 (2004), and references therein.

[48] M. Ya. Amusia, A. S. Baltenkov, L. V. Chernysheva, Z Felfli and A. Z. Msezane, J. Phys. B **38**, L169 (2005).

[49] V. K. Dolmatov and S. T. Manson, J. Phys. B **41**, 165001 (2008).

[50] V. K. Dolmatov, Adv. Quant. Chem. **58**, 13 (2009), and references therein.

[51] K. Govil, A. J. Siji, and P. C. Deshmukh, J. Phys. B **42**, 065004 (2009).

[52] J. George, H. R. Varma, P. C. Deshmukh, and S. T. Manson, J. Phys. B **45**, 185001 (2012).

[53] V. K. Dolmatov, G. T. Craven, E. Guler, and D. Keating, Phys. Rev. A **80**, 035401 (2009).

[54] V. K. Dolmatov and S. T. Manson, Phys. Rev. A **73**, 013201 (2006).

[55] Y. B. Xu, M. Q. Tan, and U. Becker, Phys. Rev. Lett. **76**, 3538 (1996).

[56] W. R. Johnson and K. T. Cheng, Phys. Rev. A **20**, 978 (1979).

[57] W. R. Johnson and K. T. Cheng, Phys. Rev. Lett. **40**, 1167 (1978).

[58] A. S. Kheifets, A. Mandal, P. C. Deshmukh, V. K. Dolmatov, D. A. Keating, and S. T. Manson, Phys. Rev. A **94**, 013423 (2016).

[59] M. Ya. Amusia and L. V. Chernysheva, *Computation of Atomic Processes: A Handbook for the ATOM Programs* (Institute of Physics, Bristol, UK, 1997).

[60] S. T. Manson, C. E. Theodosiou, and M. Inokuti, Phys. Rev. A **43**, 4688 (1991), and references therein.

[61] E. W. B. Dias, H. S. Chakraborty, P. C. Deshmukh, S. T. Manson, O. Hemmers, P. Glans, D. L. Hansen, H. Wang, S. B. Whitfield, D. W. Lindle, R. Wehlitz, J. C. Levin, I. A. Sellin, and R. C. C. Perera, Phys. Rev. Lett. **78**, 4553 (1997).

[62] D. L. Hansen, O. Hemmers, H. Wang, D. W. Lindle, P. Focke, I. A. Sellin, C. Heske, H. S. Chakraborty, P. C. Deshmukh, and S. T. Manson, Phys. Rev. A **60**, R2641 (1999).

[63] M. Ya. Amusia, N. B. Avdonina, E. G. Drukarev, S. T. Manson, and R. H. Pratt, Phys. Rev. Lett. **85**, 4703 (2000).

[64] O. Hemmers, G. Fisher, P. Glans, D. L. Hansen, H. Wang, S. B. Whitfield, D. W. Lindle, R. Wehlitz, J. C. Levin, I. A. Sellin, R. C. C. Perera, E. W. B. Dias, H. S. Chakraborty, P. C. Deshmukh, and S. T. Manson, J. Phys. B **30**, L727 (1997).

[65] V. K. Dolmatov and S. T. Manson, Phys. Rev. A **63**, 022704 (2001).

[66] J. M. Dahlström, D. Guénot, K. Klünder, M. Gisselbrecht, J. Mauritsson, A. L'Huillier, A. Maquet, and R. Taïeb, Chem. Phys. **414**, 53 (2013).